

The boring history of *Gaia* BH3 from isolated binary evolution

Giuliano Iorio^{1,2,3,*}, Stefano Torniamenti^{4,2,*}, Michela Mapelli^{4,1,2,3,*}, Marco Dall'Amico^{1,2},
Alessandro A. Trani⁵, Sara Rastello⁶, Cecilia Sgalletta^{2,7}, Stefano Rinaldi^{1,4}, Guglielmo Costa^{8,3},
Bera A. Dahl-Lahtinen¹, Gastón J. Escobar^{1,2}, Erika Korb^{1,2,4}, M. Paola Vaccaro⁴,
Elena Lacchin^{1,2,4,9}, Benedetta Mestichelli^{4,10,11}, Ugo N. Di Carlo⁷,
Mario Spera⁷, and Manuel Arca Sedda^{10,11,12}

¹ Physics and Astronomy Department Galileo Galilei, University of Padova, Vicolo dell'Osservatorio 3, 35122, Padova, Italy

² INFN – Padova, Via Marzolo 8, 35131 Padova, Italy

³ INAF – Padova, Vicolo dell'Osservatorio 5, 35122 Padova, Italy

⁴ Institut für Theoretische Astrophysik, ZAH, Universität Heidelberg, Albert-Ueberle-Straße 2, 69120 Heidelberg, Germany

⁵ Niels Bohr International Academy, Niels Bohr Institute, Blegdamsvej 17, 2100 Copenhagen, Denmark

⁶ Departament de Física Quàntica i Astrofísica, Institut de Ciències del Cosmos, Universitat de Barcelona, Martí i Franquès 1, 08028 Barcelona, Spain

⁷ SISSA, via Bonomea 365, 34136 Trieste, Italy

⁸ Univ Lyon, Univ Lyon1, ENS de Lyon, CNRS, Centre de Recherche Astrophysique de Lyon UMR5574, 69230 Saint-Genis-Laval, France

⁹ INAF, Osservatorio Astronomico di Bologna, Via Gobetti 93/3, 40129 Bologna, Italy

¹⁰ Gran Sasso Science Institute, Via F. Crispi 7, 67100 L'Aquila, Italy

¹¹ INFN – Laboratori Nazionali del Gran Sasso, 67100 L'Aquila, Italy

¹² INAF – Osservatorio Astronomico d'Abruzzo, Via Mentore Maggini, s.n.c., 64100 Teramo, Italy

Received 26 April 2024 / Accepted 31 July 2024

ABSTRACT

Gaia BH3 is the first observed dormant black hole (BH) with a mass of $\approx 30 M_{\odot}$, and it represents the first confirmation that such massive BHs are associated with metal-poor stars. Here, we explore the isolated binary formation channel for *Gaia* BH3, focusing on the old and metal-poor stellar population of the Milky Way halo. We used the MIST stellar models and our open-source population synthesis code SEVN to evolve 5.6×10^8 binaries, exploring 20 sets of parameters that encompass different natal kicks, metallicities, common envelope efficiencies and binding energies, and models for the Roche-lobe overflow. We find that systems such as *Gaia* BH3 form preferentially from binaries initially composed of a massive star ($40\text{--}60 M_{\odot}$) and a low-mass companion ($< 1 M_{\odot}$) in a wide ($P > 10^3$ days) and eccentric orbit ($e > 0.6$). Such progenitor binary stars do not undergo any Roche-lobe overflow episode during their entire evolution, so the final orbital properties of the BH-star system are essentially determined at the core collapse of the primary star. Low natal kicks ($\lesssim 10$ km/s) significantly favour the formation of *Gaia* BH3-like systems, but high velocity kicks up to ≈ 220 km/s are also allowed. We estimated the formation efficiency for *Gaia* BH3-like systems in old ($t > 10$ Gyr) and metal-poor ($Z < 0.01$) populations to be $\sim 4 \times 10^{-8} M_{\odot}^{-1}$ (for our fiducial model), representing $\sim 3\%$ of the whole simulated BH-star population. We expect up to ≈ 4000 BH-star systems in the Galactic halo formed through isolated evolution, of which ≈ 100 are compatible with *Gaia* BH3. *Gaia* BH3-like systems represent a common product of isolated binary evolution at low metallicity ($Z < 0.01$), but given the steep density profile of the Galactic halo, we do not expect more than one at the observed distance of *Gaia* BH3. Our models show that even if it was born inside a stellar cluster, *Gaia* BH3 is compatible with a primordial binary star that escaped from its parent cluster without experiencing significant dynamical interactions.

Key words. methods: numerical – binaries: general – stars: black holes – stars: massive – Galaxy: halo – Galaxy: stellar content

1. Introduction

Gaia data (Gaia Collaboration 2023) offer a unique opportunity to search for dormant black holes (BHs), that is X-ray and radio-quiet BHs that are members of a binary system with a star (Guseinov & Zel'dovich 1966; Trimble & Thorne 1969). *Gaia* BH3, the third dormant BH retrieved from these data, has a mass of $\approx 33 M_{\odot}$ and is member of a loose eccentric binary system (orbital period $P \approx 4000$ days, eccentricity $e \approx 0.72$) that includes a $\approx 0.76 M_{\odot}$ very metal-poor giant star

($[\text{Fe}/\text{H}] = -2.56 \pm 0.12$ obtained from the spectrum of the Ultraviolet and Visual Echelle Spectrograph; Gaia Collaboration 2024).

Gaia BH3 is the first-ever discovered dormant BH with a mass $\gtrsim 30 M_{\odot}$ and the first stellar BH with such a high mass unequivocally observed in the Milky Way. The other two *Gaia* BHs (BH1 and BH2) both have a mass of $\approx 10 M_{\odot}$ (El-Badry et al. 2023b,a; Chakrabarti et al. 2023; Tanikawa et al. 2024). All the other dormant BH candidates (Casares et al. 2014; Ribó et al. 2017; Giesers et al. 2018, 2019; Thompson et al. 2019; Shenar et al. 2022a,b; Mahy et al. 2022; Lennon et al. 2022; Saracino et al. 2022, 2023) and the BHs in X-ray binary systems with a dynamical measurement have a mass between a few and $\approx 20 M_{\odot}$ (Özel et al. 2010; Miller-Jones et al. 2021).

* Corresponding authors; giuliano.iorio.astro@gmail.com;
stefano.torniamenti@uni-heidelberg.de;
mapelli@uni-heidelberg.de

Stellar BHs with a mass $\gtrsim 30 M_{\odot}$ have been observed for the first time with gravitational waves (Abbott et al. 2016a,b, 2021, 2024, 2023). According to the main formation scenario, such massive BHs are expected to form from metal-poor stars, which do not lose much mass by stellar winds and collapse to a BH directly (Heger & Woosley 2002; Mapelli et al. 2009, 2010, 2013; Zampieri & Roberts 2009; Belczynski et al. 2010; Fryer et al. 2012; Ziosi et al. 2014; Spera et al. 2015). Gravitational wave data have proven the existence of such ‘oversized’ BHs, but they do not carry any information about the progenitor’s metallicity because no electromagnetic counterpart has been observed. Hence, *Gaia* BH3 is the first direct confirmation that BHs with a mass in excess of $30 M_{\odot}$ are associated with metal-poor stellar populations, thus supporting the main theoretical scenario.

For both its chemical composition and Galactic orbit, *Gaia* BH3 is associated with the ED-2 stream, which is composed of stars that are at least 12 Gyr old (Balbinot et al. 2024). Thus, this is the first BH unambiguously associated with a disrupted star cluster with a mass of 2×10^3 – $4.2 \times 10^4 M_{\odot}$ (Balbinot et al. 2024). Preliminary numerical models have shown that *Gaia* BH3 might have assembled dynamically from a low-mass star and a BH that did not evolve in the same binary star system (Marín Pina et al. 2024).

While the association of *Gaia* BH3 with the ED-2 stream is indisputable, in this work we show that this system is compatible with the nearly unperturbed evolution of a primordial binary star. Our population-synthesis simulations show that we do not need to invoke a dynamical exchange or a dynamical capture to explain its orbital properties.

Gaia BH3 is very different from both *Gaia* BH1 and *Gaia* BH2, which challenge our models of binary evolution (El-Badry et al. 2023b,a; Chakrabarti et al. 2023; Tanikawa et al. 2023; Rastello et al. 2023; Di Carlo et al. 2024; Generozov & Perets 2024, but see Kotko et al. 2024). The wide orbital separation of *Gaia* BH3 does not require evolution via Roche-lobe overflow or a common envelope. Rather, it is consistent with a wide system that never went through mass transfer and survived the formation of the BH because it happened via an almost direct collapse with a mild natal kick.

In this work, we show that the measured orbital eccentricity helps constrain the phase of the binary at the time of the formation of the BH. This paper is organised as follows. We describe our methodology in Sect. 2, present the main results in Sect. 3, and discuss the implications in Sect. 4. Section 5 provides a summary of our main takeaways.

2. Methods

In this work, we compare the observational features of the *Gaia* BH3 system with a synthetic population of stellar binaries produced with the Stellar EVolution for N-body (SEVN) code¹ (Spera & Mapelli 2017; Spera et al. 2019; Mapelli et al. 2020; Iorio et al. 2023). In SEVN, the evolution of single stars is estimated by interpolating on the fly across pre-calculated stellar evolution tracks stored in custom lookup tables. The models presented in this study were computed using the MIST stellar tracks by Choi et al. (2016). We used TRACKCRUNCHER²

¹ In this work, we used the SEVN version V 2.10.1 (commit a4753f11) publicly available at the GitLab repository <https://gitlab.com/sevncodes/sevn>

² The version of the code we used to produce the tables is available at <https://gitlab.com/sevncodes/trackcruncher> (commit 0827337).

(Iorio et al. 2023) to produce the SEVN tables from the MIST stellar tracks. We produced eight sets of tables from metallicity $Z = 1.4 \times 10^{-5}$ to 4.5×10^{-2} ; each set contains stellar tracks from $0.71 M_{\odot}$ to $150 M_{\odot}$.

In SEVN, binary interactions are described through analytical and semi-analytical prescriptions, encompassing stable mass transfer by Roche-lobe overflow and winds, common envelope evolution, angular momentum dissipation by magnetic braking, tidal interactions, orbital decay by gravitational-wave emission, dynamical hardening, chemically homogeneous evolution, and stellar mergers. In our models, we treated tidal forces with the analytical formalism developed by Hut (1981) and as implemented by Hurley et al. (2002). For more details, we refer to Iorio et al. (2023).

2.1. Initial conditions

We generated the initial conditions for 2×10^7 binary systems by extracting the zero-age main-sequence mass of the primary (more massive) star, m_1 , from the Kroupa initial mass function (Kroupa 2001) from 5 to $150 M_{\odot}$. The mass of the secondary (less massive) star was set from the binary mass ratio q following the distribution $\text{PDF}(q) \propto q^{-0.1}$ with $q \in [0.71 M_{\odot}/m_1, 1]$. We obtained the initial orbital period (P) and eccentricity (e) from the following distributions: $\text{PDF}(\log P/\text{days}) \propto (\log P)^{-0.55}$, $\text{PDF}(e) \propto e^{-0.42}$. These distributions of mass ratios, orbital periods, and eccentricities represent the best fits to observations of massive binary stars in Galactic young clusters (Sana et al. 2012). The periods range from 1.4 days to 866 years, while the eccentricities range from 0 to $e_{\text{max}} = 1 - (P/2 \text{ days})^{-2/3}$, according to Moe & Di Stefano (2017). The total mass of the simulated population is $M_{\text{sim}} = 4.2 \times 10^8 M_{\odot}$, corresponding to a mass of $M_{\text{tot}} = 1.4 \times 10^9 M_{\odot}$ (roughly equivalent to the mass of the Galactic stellar halo; see Deason et al. 2019) when accounting for the fact that we did not simulate low-mass primary stars and systems with secondary stars less massive than $0.71 M_{\odot}$ ³. We used SEVN to evolve all the generated binaries from the zero age main sequence up to the moment in which the two stars are compact remnants (white dwarfs, neutron stars, BHs). The files of the initial conditions and parameters are publicly available in Zenodo⁴.

2.2. Fiducial model

In our fiducial model, we used the default SEVN options as described by Iorio et al. (2023) (see also Sgalletta et al. 2023; Costa et al. 2023) except for the circularisation option. Here, we used the new default circularisation option *angmom*, in which at the onset of the Roche-lobe overflow the orbit is circularised, conserving the angular momentum so that the new semi-major axis is $a_{\text{new}} = a_{\text{old}}(1 - e_{\text{old}}^2)$.

The stability of the Roche-lobe mass transfer is checked by comparing the current binary mass ratio to a critical mass ratio that depends on the stellar evolutionary phase. In this work, we used the default option of SEVN (Iorio et al. 2023) in which the Roche-lobe overflow episodes involving stars with a radiative envelope (main-sequence stars and low-mass stars before climbing the red giant branch) are always stable, while in all the other cases we used the value of the critical mass ratio by

³ We assumed a parent population with primary masses m_1 between $0.08 M_{\odot}$ and $150 M_{\odot}$ and mass ratios in the range $q \in [0.08 M_{\odot}/m_1, 1]$.

⁴ [10.5281/zenodo.11617742](https://zenodo.org/record/11617742)

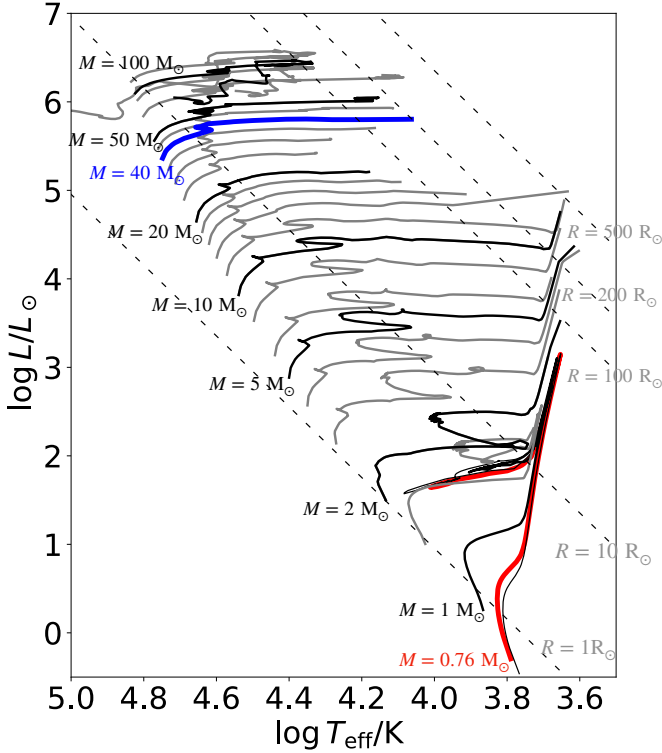


Fig. 1. Hertzsprung–Russell diagram of a sample of stars at metallicity $Z = 4.1 \times 10^{-5}$ interpolated by SEVN from the MIST stellar tracks. The blue and red lines respectively show the likely progenitors of the BH and stellar companion in *Gaia* BH3.

Hurley et al. (2002). When the mass transfer is unstable, a common envelope evolution phase begins (Ivanova et al. 2013). We used the standard $\alpha - \lambda$ prescription for the common envelope (Webbink 1984; Hurley et al. 2002, and references therein) with the ejection efficiency parameter $\alpha = 1$, whereas we estimated λ using the formalism by Claeys et al. (2014) and as implemented in SEVN (see Appendix A1.4 in Iorio et al. 2023).

After a core-collapse supernova, we decided the mass of the BH based on the delayed model by Fryer et al. (2012). We adopted the supernova kick model by Giacobbo & Mapelli (2020), where the natal kick is drawn from a Maxwellian distribution with a one-dimensional root-mean-square $\sigma_{\text{rms}} = 265$ km/s (Hobbs et al. 2005), re-scaled by the ejecta mass and the compact-remnant mass and resulting in a much lower ($\lesssim 10$ km/s) effective kick for the massive BHs ($> 30 M_{\odot}$).

In the fiducial model, we set the metallicity to $Z = 4.1 \times 10^{-5}$, which corresponds to the observed value of $[\text{Fe}/\text{H}] = -2.56$ when considering the MIST stellar models. The MIST stellar tracks with the fiducial metallicity are shown in Fig. 1.

2.3. Additional models: Parameter-space exploration

To explore the parameter space for the formation of *Gaia* BH3-like systems, we ran an additional set of 17 simulations varying one parameter of the fiducial simulation per time and two additional sets varying the initial conditions. For the initial conditions, we used the same set of 2×10^7 binary systems as for the fiducial model.

We simulated eight additional metallicities: $Z = 0.0001$ (model Z1E-4), $Z = 0.0004$ (model Z4E-4), $Z = 0.0008$ (model

Z8E-4), $Z = 0.001$ (model Z1E-3), $Z = 0.004$ model (Z4E-3), $Z = 0.006$ (model Z6E-3), $Z = 0.008$ (model Z8E-3), and $Z = 0.01$ (model Z1E-2). We also explored the effect of the supernova kick by running four different simulations in which the kicks are drawn from a Maxwellian distribution with $\sigma_{\text{rms}} = 1$ km/s (essentially no kick, model VK1), 50 km/s (VK50), 100 km/s (VK100), and 265 km/s (VK265). In these models, the kick is not re-scaled for the ejected mass and the mass of the compact remnant. We also tested the importance of the common-envelope phase by running two simulations varying the common envelope efficiency ($\alpha = 3$, model CE α 3, and $\alpha = 5$, model CE α 5) and two additional simulations varying the binding energy formalism (model CE λ XL10 using the fitting equations by Xu & Li 2010 and model CE λ K21 using the fitting equations by Klencki et al. 2021⁵). Furthermore, we ran an additional model (RLOp) in which we allowed the system to start a Roche-lobe overflow in an eccentric orbit if the condition of Roche-lobe overflow is satisfied at the periastron, that is, if the stellar radius is larger than $R_L = r_{\text{peri}} f(q)$, where r_{peri} is the periastron and $f(q)$ is a function that depends on the binary mass ratio (Eggleton 1983).

Since *Gaia* BH3 is an eccentric system, we also ran an additional simulation (model ICthermal) to examine the impact of the initial eccentricity distribution. In this simulation, the initial orbital eccentricity is drawn from a thermal distribution, which favours eccentric systems, $\text{PDF}(e) \propto e$ (see e.g. Geller et al. 2019).

Finally, to assess the uncertainties due to the initial condition sampling, we drew an additional set of 1.8×10^8 binaries and simulated their evolution using the same setup as the fiducial simulation. We combined the results of the additional simulations with those from the fiducial simulation, and labeled the final combined dataset as ‘fiducial2E8’. The total mass evolved in this case is $M_{\text{sim}} = 4.2 \times 10^9 M_{\odot}$, corresponding to a total population mass of $M_{\text{tot}} = 1.4 \times 10^{10} M_{\odot}$ (see Sect. 2.2). The results of the simulations are publicly available in Zenodo.

3. Results

Figure 2 shows the properties of the BH-star systems in the fiducial model. We considered all the simulation outputs in which a binary system is composed of a BH and a giant star, that is, a star that left the main sequence and has not started the core helium burning phase yet. We imposed the additional condition that the system is not undergoing a common-envelope or Roche-lobe overflow episode. The colour map of Fig. 2 represents the time spent by all the systems in such a configuration, which is a proxy of the likelihood of observing a given system.

Binaries hosting a BH and a massive companion are, in general, more common in the simulations, but the short lifetime of

⁵ In SEVN version 2.10.0, we revised the implementation of the λ_{K21} fitting equations by Klencki et al. 2021. We corrected a bug in the code that affected the λ_{K21} estimate for metallicities $Z < 0.017$ (the bug has been fixed for all the versions greater than 2.8.0). Additionally, we improved the fit for cases in which the stellar radius is less than the radius at the terminal age main sequence (TAMS) of the MESA stellar tracks used in Klencki et al. (2021) (private communication). In this radial range, the original fitting equations were extrapolated, leading to high binding energies ($> 10^{52}$ ergs). For additional information, we refer to the discussion in the SEVN repository: <https://gitlab.com/sevncodes/sevn/-/issues/4>

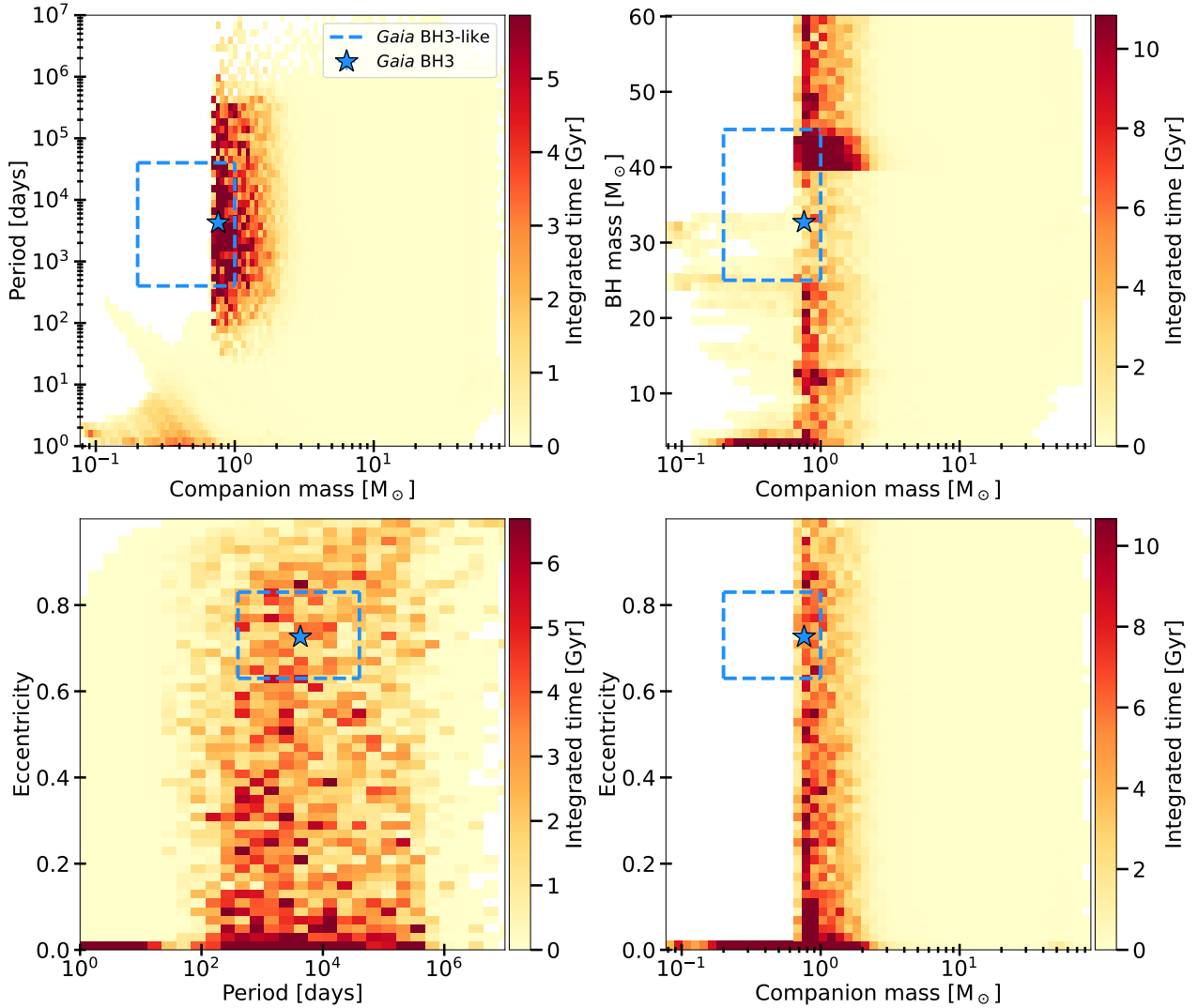


Fig. 2. Properties of non-interacting BH-star systems in the fiducial model. Here, we only show stars in the giant phase, that is, outside the main sequence and that have not started the core helium burning phase yet. Also, we do not show systems that undergo a Roche-lobe overflow episode. From top to bottom and from left to right: Orbital period versus companion star mass; BH mass versus companion star mass; eccentricity versus orbital period; eccentricity versus companion star mass. The colour map shows the integrated time spent by the systems in a given bin; thus, it is a proxy of the likelihood of observing a system with such properties. The map does not include information about the stellar luminosity, which is also important for detectability. We assumed a metallicity of $Z = 4.1 \times 10^{-5}$. The star indicates the properties of *Gaia* BH3, while the light blue boxes show the criteria used to select *Gaia* BH3-like systems. The colour maps saturate at 98% of the maximum value.

the massive star makes them less likely to be observed. In contrast, BH–low-mass star binaries are rarer, but once formed, they can remain in the same configuration for several gigayears.

Gaia BH3 is located in a region of the parameter space well covered by the fiducial simulation, especially when considering binary systems older than 10 Gyr. In addition, the *Gaia* BH3 properties (mostly period and BH mass) cover a range in which *Gaia* is particularly sensitive to astrometric signals of binarity (see e.g. Penoyre et al. 2022). From Fig. 2, we can conclude that if a BH-star system is observed in an old and metal-poor population, it is not surprising to find it with the *Gaia* BH3 configuration. In this sense, *Gaia* BH3 is not an outlier, unlike *Gaia* BH1 and BH2 (El-Badry et al. 2023b; Rastello et al. 2023).

It is convenient to define a region of the observed parameter space to identify *Gaia* BH3-like systems. For the sake of simplicity and to help the comparison with previous work, we used a selection cut similar to the one used in Marín Pina et al. (2024): $P \in [400, 40\,000]$ days, $m_s \in [0.2, 1]$ M_\odot ,

$m_{\text{bh}} \in [25, 45]$ M_\odot , $e \in [0.63, 0.83]$. The box represents about 1% of the volume of the parameter space that includes BH-star systems at ages older than 10 Gyr.

3.1. Formation history

All the *Gaia* BH3-like systems in our models have the same simple formation history. Their progenitors consist of a massive star ($>40 M_\odot$) and a low-mass companion ($<1 M_\odot$). The binary components never interact through Roche-lobe overflow, so the orbital properties at BH formation are almost the same as their initial ones. The final properties of the BH-star system are thus determined by the binary phase at the moment of the supernova explosion, the amount of mass lost during the evolution, and the BH natal kick.

In our fiducial model, the initial BH progenitor mass is about 40–50 M_\odot , and the ejected mass at BH formation is 10–20 M_\odot . The mild BH natal kick (<10 km/s) cannot drastically change

the binary orbital parameters. As a consequence, a large majority of BH progenitors originated with orbital properties very similar to *Gaia* BH3, namely, a period between 10^3 and 10^4 days and an eccentricity in the range 0.6–0.9. The system more similar to *Gaia* BH3 has an initial period of about 1500 days, an eccentricity of 0.65, a stellar mass of $0.83 M_{\odot}$, and an initial BH progenitor mass of $41 M_{\odot}$. We found a sub-population (<10% of the total) that produces *Gaia* BH3-like systems starting from almost circular orbits ($e < 0.2$) and lower initial periods (< 10^3 days). For these systems, the final orbital properties are determined by the high value of the BH natal kick. A few systems ($\approx 3\%$) have very massive BH progenitors of about $120 M_{\odot}$ that produce BHs with a mass of $\sim 30 M_{\odot}$ because of mass loss during pulsational pair instability (Heger & Woosley 2002; Belczynski et al. 2016; Woosley 2017, 2019; Farmer et al. 2019; Costa et al. 2021; Tanikawa et al. 2021).

In all of our models, the progenitors of *Gaia* BH3 do not undergo any (stable or unstable) mass transfer episode. Therefore, there are no differences among the models CE α 3, CE α 5, CE λ XL10, and CE λ K21. Also, we found only a mild decrease in the number of *Gaia* BH3-like systems for the model RLOp, which indicates that including or not including the possibility to trigger a stable mass transfer at periastron is not important for the production of such binary systems. We found the same progenitors in the case of the kick model VK1, which serves as confirmation that in the fiducial model, the implemented kick model produces very low kicks for the case of *Gaia* BH3-like progenitors.

Models with higher kick velocities show significant differences in the initial orbital properties. The BH natal kicks in models VK50 and VK100 are able to wash out any correlation between the initial and final period and eccentricity. The *Gaia* BH3-like progenitors have initial periods and eccentricities almost uniformly distributed in the range 100–4000 days and 0–0.8, respectively. At very high velocities (model VK265), the formation of *Gaia* BH3-like binaries is strongly suppressed. Most systems break during BH formation, and just a few of them (four out of the 20 million simulated binaries) had a lucky configuration of binary phase and/or velocity kick that let them survive the supernova event.

We found a trend with metallicity for the initial orbital period, eccentricity, and BH progenitor mass. From low metallicity (model Z1E-4) to intermediate-high metallicity (model Z1E-2), the lower limit of the initial period moves toward higher values ($P > 1000$ days for model Z1E-2), while the sub-populations with initial low eccentricity ($e < 0.6$) tend to disappear. As for the BH progenitor mass, the range of values widens with increasing metallicity, up to initial masses of $100 M_{\odot}$. This is due to the non-monotonic trend of the initial BH mass relation of the MIST tracks used in this work when paired with the rapid and delayed supernova models by Fryer et al. (2012). When assuming initial masses lower than $60 M_{\odot}$, the combination of the Fryer et al. (2012) supernova models and the MIST tracks produces BHs more massive than 25 and $30 M_{\odot}$ up to a metallicity $Z = 0.02$ and 0.01, respectively. When relaxing the limit on the initial masses, BHs more massive than $30 M_{\odot}$ are excluded only for $Z > 0.02$.

Mass transfer through stellar winds is negligible ($< 10^{-9} M_{\odot}$) in all of the simulated *Gaia* BH3-like objects. At BH formation, a typical *Gaia* BH3 progenitor hosts a low-mass star with stellar radius $R_* < 1 R_{\odot}$ at a distance from the supernova explosion of $D_{\text{sn}} = 1000\text{--}4000 R_{\odot}$. Considering a total ejected mass of $M_{\text{ej}} = 10 M_{\odot}$, the amount of mass deposited into the low-mass companion is $< M_{\text{ej}} R_*^2 / D_{\text{sn}}^2 \sim 10^{-5}\text{--}10^{-6} M_{\odot}$. As discussed by

El-Badry (2024), this amount of pollution is hardly detectable in the spectral lines. In addition, the MIST models predict that a $\sim 0.8 M_{\odot}$ star loses $10^{-2}\text{--}10^{-3} M_{\odot}$ from the main-sequence to the red giant phase, likely removing all the material deposited from the supernova into the star external layer. In conclusion, we do not expect any peculiar chemical signature in the *Gaia* BH3 star if it formed through the isolated channel. This is consistent with the observations (Gaia Collaboration 2024).

3.2. Bayesian sampling

The SEVN simulations indicate that the region of *Gaia* BH3 in the observed parameter space (P , e , m_{BH} , m_{ms}) tends to be populated by systems in which the binary components never interact. Therefore, the final binary properties are determined by the initial binary parameters and the details of the BH formation only. In order to focus on *Gaia* BH3 progenitors independently of the chosen selection cut, we implemented a simple Bayesian sampling technique in which we sample the posteriors of the binary initial conditions. We assume the likelihood is a multivariate normal distribution centred on the *Gaia* BH3 values and with the standard deviations equal to the reported errors (which we assumed to be independent).

For the parameter priors, we used:

- a uniform distribution for the mean anomaly (between 0 and 2π) at the moment of the BH formation,
- a uniform distribution for the mass of the BH progenitor between 20 and $100 M_{\odot}$,
- a uniform distribution for eccentricity between 0 and 1,
- a log-uniform distribution for the period between 10 and 10^6 days,
- a normal distribution for the three spherical components of the velocity kick, corresponding to a Maxwellian distribution of the velocity module.

For the velocity distribution, we tested five different values of the one-dimensional root-mean-square velocity for the Maxwellian distribution (1, 10, 50, 100, 256 km/s). We also excluded the interacting binary systems by setting the prior to be equal to zero when the maximum radius of the BH progenitor is larger than either the separation at periastron or the Roche-lobe radius at periastron (see Sect. 2). To estimate the final properties of the binary, we used the formalism in the appendix of Hurley et al. (2002), and we estimated the maximum radius and the final mass of the BH progenitor by using SEVN. The posteriors were sampled using the Monte Carlo Markov chain (MCMC) ensemble sampler available in the ‘emcee’ python package (Foreman-Mackey et al. 2013). This method is similar to the grid search presented by El-Badry (2024), but our method is tailored to exactly reproducing the observed properties of *Gaia* BH3. Since we included the reduction of the parameter space due to stellar interactions directly in the priors, the posteriors do not need to be corrected a posteriori.

We show the posterior samples in Fig. 3. Overall, they are consistent with what was obtained from the SEVN simulations for the wider space of the selection cut assumed in Sect. 3.1. Assuming low kick velocities, the *Gaia* BH3 progenitor is very likely to have originated from a wide and eccentric binary ($P \approx 3500$ days, $e \sim 0.75$). The smaller peak at around 10^3 days and $e \sim 0.4$ is due to systems that form the BH at periastron, where it is more favourable to produce large final eccentricities due to the impact of mass loss during the supernova explosion. Larger kicks widen the range of initial periods and eccentricities, with most of the initial periods being around 500–600 days. The period distribution is sharply cut below 300 days because the objects

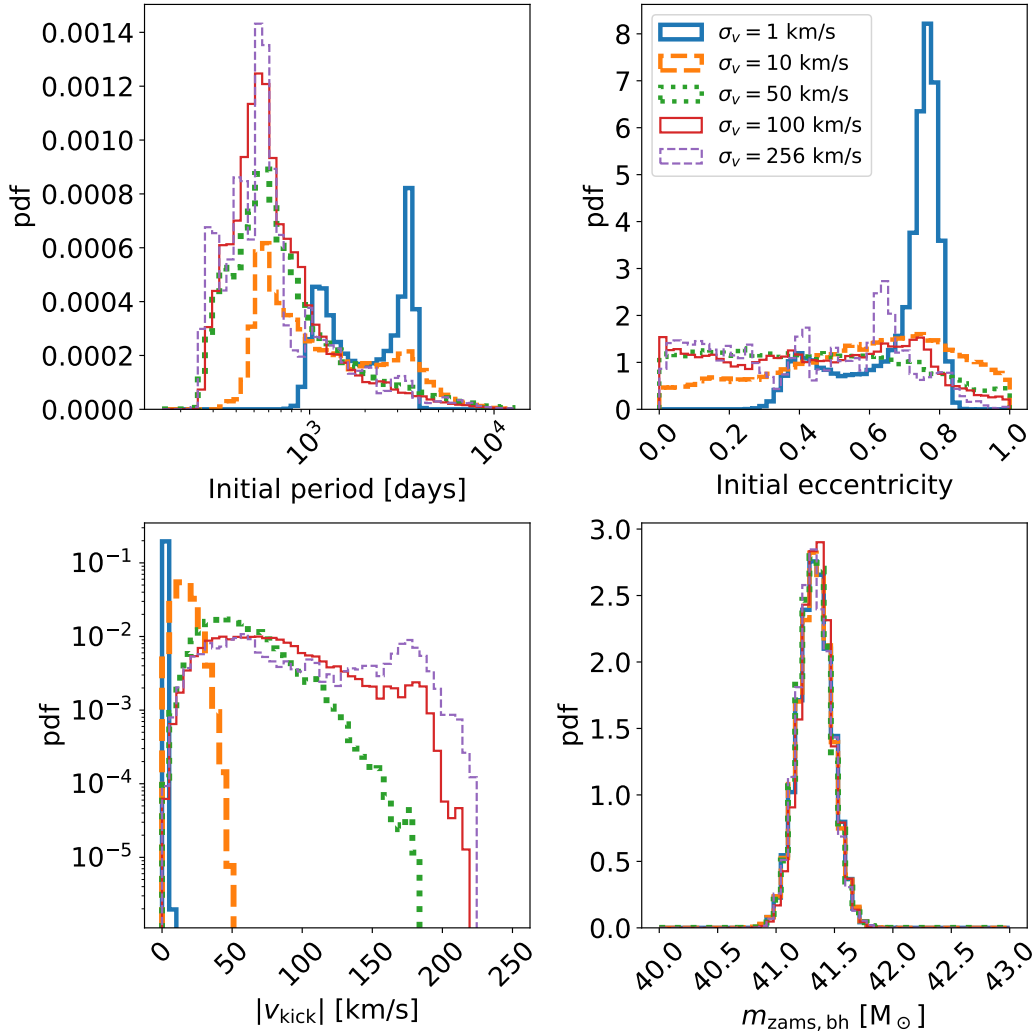


Fig. 3. Distribution of the initial conditions of the binaries that reproduce the *Gaia* BH3 properties after BH formation. From top left to bottom right, the panels show the initial binary period, initial eccentricity, the module of the BH natal kick velocity, and the initial mass of the BH progenitor. We show the distributions obtained assuming different Maxwellian-distribution priors for the kick velocity: $\sigma_v = 1$ km/s (blue thick solid line), $\sigma_v = 10$ km/s (orange thick dashed line), $\sigma_v = 50$ km/s (green dotted line), $\sigma_v = 100$ km/s (red thin solid line), $\sigma_v = 256$ km/s (violet thin dashed line).

are tight enough to interact. It is possible to form a *Gaia* BH3 system with initial kicks up to 200 km/s. For higher values, the kick is larger than the escape velocity at periastron in the whole range of periods that are consistent with a non-interacting binary.

Independent of the explored parameters, a clear picture emerged. In the presence of low supernova kicks (< 10 km/s), *Gaia* BH3-like systems form from non-interacting binary progenitors preferentially in a wide ($500 < P/\text{days} < 2 \times 10^4$) and eccentric configuration. Alternatively, on the off chance that the binary survives to higher supernova kicks, systems with *Gaia* BH3 properties can form preferentially from tighter ($P/\text{days} \sim 500$) systems almost independently of their initial eccentricity if $e < 0.7$. For this reason, the initial properties of the binary can play a key role in setting the formation efficiency of *Gaia* BH3-like systems. Indeed, the model with a higher initial eccentricity (ICthermal) produces two to three times more *Gaia* BH3-like systems compared to our fiducial run (Table 1).

3.3. Halo population

In the explored models, *Gaia* BH3-like systems represent one of the standard outcomes of binary evolution. Next, we

investigated how common *Gaia* BH3-like systems and BH-star binaries are in the Galactic halo environment, which is characterised by low metallicity and old ages. We also assumed $t > 10$ Gyr. First, we estimated the formation efficiency, defined as the ratio of the number of objects to the total simulated mass. We corrected the total mass in the initial conditions for the incomplete mass sampling of the primary, and we assumed an initial binary fraction of one for the sake of simplicity. Table 1 reports the formation efficiency of all the systems in the *Gaia* BH3 selection box (Fig. 2) as well as of those systems that are in the selection box and in the BH-star configuration after 10 Gyr.

In the fiducial model, the population of *Gaia* BH3-like objects accounts for about 2–3% of the whole population at $t > 10$ Gyr. This number is consistent with the volume fraction sampled by the selection box. Models with higher kicks significantly suppress the formation of both *Gaia* BH3-like and BH-star systems, while a higher metallicity increases their formation efficiency up to a factor of two. Given the formation history of *Gaia* BH3-like objects, the efficiency is not affected by the choice of the common-envelope ejection efficiency and binding energy. However, larger values of the common envelope

Table 1. Formation efficiency (M_{\odot}^{-1}) for *Gaia* BH3-like and BH-star systems obtained from different simulation models.

Model	η_{Gaia} BH3-like	η_{Gaia} BH3-like ($t > 10$ Gyr)	η_{Gaia} BH3-like ($t > 10$ Gyr) ($v_{sys} < 10$ km s $^{-1}$)	η_{Gaia} BH3-like ($t > 10$ Gyr) ($v_{sys} < 1$ km s $^{-1}$)	$\eta_{BH-star}$ ($t > 10$ Gyr)
fiducial	$(9.7 \pm 0.8) \times 10^{-8}$	$(3.9 \pm 0.5) \times 10^{-8}$	$(2.8 \pm 0.4) \times 10^{-8}$	$(2.5 \pm 0.4) \times 10^{-8}$	$(1.6 \pm 0.1) \times 10^{-6}$
fiducial2E8	$(1.0 \pm 0.1) \times 10^{-7}$	$(4.4 \pm 0.2) \times 10^{-8}$	$(3.5 \pm 0.2) \times 10^{-8}$	$(3.0 \pm 0.2) \times 10^{-8}$	$(1.6 \pm 0.1) \times 10^{-6}$
ICthermal	$(2.4 \pm 0.1) \times 10^{-7}$	$(1.0 \pm 0.1) \times 10^{-7}$	$(9.0 \pm 0.8) \times 10^{-8}$	$(7.8 \pm 0.7) \times 10^{-8}$	$(1.3 \pm 0.1) \times 10^{-6}$
RLOp	$(9.1 \pm 0.8) \times 10^{-8}$	$(3.5 \pm 0.5) \times 10^{-8}$	$(2.5 \pm 0.4) \times 10^{-8}$	$(2.3 \pm 0.4) \times 10^{-8}$	$(1.6 \pm 0.1) \times 10^{-6}$
VK1	$(1.0 \pm 0.1) \times 10^{-7}$	$(3.9 \pm 0.5) \times 10^{-8}$	$(3.9 \pm 0.5) \times 10^{-8}$	$(8.5 \pm 0.2) \times 10^{-9}$	$(2.3 \pm 0.1) \times 10^{-6}$
VK50	$(9.0 \pm 0.8) \times 10^{-8}$	$(4.0 \pm 0.5) \times 10^{-8}$	0	0	$(9.0 \pm 0.3) \times 10^{-7}$
VK100	$(3.6 \pm 0.5) \times 10^{-8}$	$(1.1 \pm 0.3) \times 10^{-8}$	0	0	$(6.0 \pm 0.2) \times 10^{-7}$
VK265	$(6.4 \pm 2.1) \times 10^{-9}$	$(2.1 \pm 1.2) \times 10^{-9}$	0	0	$(6.2 \pm 0.2) \times 10^{-8}$
CE α 3	$(9.7 \pm 0.8) \times 10^{-8}$	$(3.9 \pm 0.5) \times 10^{-8}$	$(2.8 \pm 0.4) \times 10^{-8}$	$(2.5 \pm 0.4) \times 10^{-8}$	$(2.5 \pm 0.1) \times 10^{-6}$
CE α 5	$(9.7 \pm 0.8) \times 10^{-8}$	$(3.9 \pm 0.5) \times 10^{-8}$	$(2.8 \pm 0.4) \times 10^{-8}$	$(2.5 \pm 0.4) \times 10^{-8}$	$(2.8 \pm 0.1) \times 10^{-6}$
CE λ XL10	$(9.7 \pm 0.8) \times 10^{-8}$	$(3.9 \pm 0.5) \times 10^{-8}$	$(2.8 \pm 0.4) \times 10^{-8}$	$(2.5 \pm 0.4) \times 10^{-8}$	$(1.4 \pm 0.1) \times 10^{-6}$
CE λ K21	$(9.7 \pm 0.8) \times 10^{-8}$	$(3.9 \pm 0.5) \times 10^{-8}$	$(2.8 \pm 0.4) \times 10^{-8}$	$(2.5 \pm 0.4) \times 10^{-8}$	$(1.4 \pm 0.1) \times 10^{-6}$
Z1E-4	$(1.3 \pm 0.1) \times 10^{-7}$	$(4.8 \pm 0.6) \times 10^{-8}$	$(3.0 \pm 0.5) \times 10^{-8}$	$(2.7 \pm 0.4) \times 10^{-8}$	$(1.4 \pm 0.1) \times 10^{-6}$
Z4E-4	$(1.1 \pm 0.1) \times 10^{-7}$	$(4.8 \pm 0.6) \times 10^{-8}$	$(2.1 \pm 0.4) \times 10^{-8}$	$(1.7 \pm 0.3) \times 10^{-8}$	$(1.4 \pm 0.1) \times 10^{-6}$
Z8E-4	$(9.4 \pm 0.8) \times 10^{-8}$	$(3.9 \pm 0.5) \times 10^{-8}$	$(1.8 \pm 0.4) \times 10^{-8}$	$(1.4 \pm 0.3) \times 10^{-8}$	$(1.5 \pm 0.1) \times 10^{-6}$
Z1E-3	$(9.2 \pm 0.8) \times 10^{-8}$	$(4.0 \pm 0.5) \times 10^{-8}$	$(2.1 \pm 0.4) \times 10^{-8}$	$(1.9 \pm 0.4) \times 10^{-8}$	$(1.6 \pm 0.1) \times 10^{-6}$
Z4E-3	$(9.1 \pm 0.8) \times 10^{-8}$	$(5.3 \pm 0.6) \times 10^{-8}$	$(2.8 \pm 0.5) \times 10^{-8}$	$(2.1 \pm 0.4) \times 10^{-8}$	$(2.4 \pm 0.1) \times 10^{-6}$
Z6E-3	$(9.4 \pm 0.8) \times 10^{-8}$	$(5.8 \pm 0.6) \times 10^{-8}$	$(3.9 \pm 0.5) \times 10^{-8}$	$(2.8 \pm 0.4) \times 10^{-8}$	$(2.7 \pm 0.1) \times 10^{-6}$
Z8E-3	$(8.2 \pm 0.8) \times 10^{-8}$	$(6.2 \pm 0.7) \times 10^{-8}$	$(4.7 \pm 0.6) \times 10^{-8}$	$(3.3 \pm 0.5) \times 10^{-8}$	$(3.1 \pm 0.1) \times 10^{-6}$
Z1E-2	$(8.2 \pm 0.8) \times 10^{-8}$	$(7.1 \pm 0.7) \times 10^{-8}$	$(7.0 \pm 0.7) \times 10^{-8}$	$(5.9 \pm 0.6) \times 10^{-8}$	$(3.4 \pm 0.1) \times 10^{-6}$

Notes. Column 1: model name; Column 2: formation efficiency of all *Gaia* BH3-like systems, as defined by the section cut (Sect. 3); Col. 3: same as Col. 2 but with the additional condition that the system is still in the BH-star configuration after 10 Gyr; Col. 4 (5): same as Col. 3 but with the additional condition that the binary has a systemic velocity of $v_{sys} < 10$ km/s ($v_{sys} < 1$ km/s); Col. 6: all BH-star systems with an age > 10 Gyr. To calculate the formation efficiency, we assumed a 100% binary fraction. The errors are estimated as the square root of the counts over the total mass.

efficiency parameter α slightly increase the formation efficiency of the whole BH-star systems, resulting in a lower fraction of *Gaia* BH3-like systems.

Even if the Galactic stellar halo is the least massive component of our Galaxy, the most recent estimates revise its mass from a few $10^8 M_{\odot}$ (see, e.g., Bell et al. 2008) up to $0.7\text{--}1.2 \times 10^9 M_{\odot}$ (Deason et al. 2019; Lane et al. 2023). Combining the total halo mass with the formation efficiencies in Table 1, we predict the number of BH stars in the halo to be in the range of $\approx 1000\text{--}4000$. Among these systems, about 20–120 fall in the *Gaia* BH3 selection cut used in this work (Fig. 2). The Galactic stellar halo is a diffuse component extended up to 100 kpc with a steep density profile ($\rho \propto r^{-\gamma}$, with $2 < \gamma < 5$; see, e.g., Medina et al. 2024; Iorio et al. 2018 and references therein).

Deason et al. (2019) report a local density profile at the Sun location of $\rho_{h,\odot} \approx 8 \times 10^4 M_{\odot}/\text{kpc}^3$. Multiplying this density by the formation efficiencies of the old BH-star binaries, we obtained a local density of $n_{BHStar} = \eta_{BHStar} \rho_{h,\odot}$ ranging from 0.1 to 0.3 kpc^{-3} . The values correspond to an expected number of objects between 0.13 and 0.27 at the distance of *Gaia* BH3 (≈ 0.6 kpc). At face value, we do not expect any BH-star binary system from the halo in the solar neighbourhood. However, we can account for the statistical noise by assuming that the number of systems follows a Poissonian distribution with the rate λ_{BHStar} ranging between 0.13 and 0.27. In this case, the probability to observe at least one object is between 12% and 25%. By simply using the formation efficiency for the old systems in the *Gaia* BH3 selection box (Fig. 2), we obtained a Poisson rate between 0.003 and 0.006, corresponding to a

probability of observing at least one *Gaia* BH3-like system of 0.3–0.6%. Although these numbers correspond to the very low probability tail of the distribution, they cannot be rejected at the 3σ level. However, a single future detection of another *Gaia* BH3-like binary system in the Galactic halo within the solar neighbourhood would be enough to significantly rule out the isolated formation channel, according to the models presented in this work. However, this will also represent a challenge for the alternative dynamical formation channel (see Sect. 4.4).

3.4. Populations in the stellar clusters and cold structures

Balbinot et al. (2024) show that *Gaia* BH3 is associated with the ED-2 stellar stream. The presence of *Gaia* BH3-like systems in star clusters and kinematically cold structures, such as a stellar stream, pose additional constraints on the natal kick velocity in the binary centre of mass, v_{sys} . In fact, if the kick velocity is significantly larger than the typical velocity dispersion of the host cluster or stream, the BH will escape from the system and join the field population in the Milky Way. The escape velocity from globular clusters ranges from ~ 10 km s $^{-1}$ km to ~ 50 km s $^{-1}$ (Gnedin et al. 2002). Almost all ($> 90\%$) the *Gaia* BH-3 systems in our simulations have $v_{sys} < 50$ km s $^{-1}$, except for models VK50, VK100, and VK265 (Fig. 3).

Focusing on the low-velocity tail of the kick distribution, Table 1 reports the formation efficiency of *Gaia* BH3-like systems when we apply the additional selection cut of $v_{sys} < 10$ km s $^{-1}$ (typical velocity dispersion of globular clusters) and $v_{sys} < 1$ km s $^{-1}$ (drift velocity of the ED-2 components

with respect to the progenitor cluster; [Marín Pina et al. 2024](#)). For most of our models, the formation efficiency decreases by $\leq 20\text{--}30\%$. Although the effect is not negligible, the formation efficiency decrease is not significant enough to rule out the isolated formation channel for *Gaia* BH3-like systems at a 3σ level.

4. Discussion

4.1. Stellar evolution models

Uncertainties about massive star evolution have an important impact on our results. For instance, differences in the maximum radius of the BH progenitor are crucial to selecting which objects interact during binary evolution.

[El-Badry \(2024\)](#) explored the main uncertainties about stellar evolution models, concluding that most models predict that the progenitor of *Gaia* BH3 reached radii up to $1000 R_{\odot}$. Such stars cannot avoid interaction before BH formation. For this reason, [El-Badry \(2024\)](#) conclude that dynamical interactions in a star cluster represent the only possible formation channel for *Gaia* BH3, unless the radius of the BH progenitor did not exceed $\approx 700 R_{\odot}$. In our stellar evolution models based on the MIST tracks ([Choi et al. 2016](#)), the BH progenitor reaches a maximum radius of $\lesssim 200\text{--}300 R_{\odot}$ for $Z < 0.0002$ (Fig. 1). We find similar results for the PARSEC stellar tracks ([Bressan et al. 2012](#); [Chen et al. 2015](#); [Costa et al. 2021](#); [Nguyen et al. 2022](#)) available in SEVN ([Iorio et al. 2023](#)). While a detailed analysis of the differences in stellar evolution models is beyond the scope of this paper (see, e.g., [Agrawal et al. 2020, 2022a,b](#); [Klencki et al. 2020](#); [Gilkis et al. 2021](#)), it is still crucial to note their significant impact on the interpretation of *Gaia* BH3 and other BH-star systems.

4.2. Initial eccentricity and stellar tides

In all the simulations assuming our fiducial kick model ([Giacobbo & Mapelli 2020](#)), *Gaia* BH3-like systems form preferentially from binary systems with an initial eccentric orbit ($e > 0.6$). Therefore, we expect that initial distributions that favour eccentric orbits, such as the thermal distribution, boost the number of *Gaia* BH3-like systems (model ICthermal; see Table 1). In contrast, circular orbits significantly suppress the formation of such systems unless high kick models are used.

In some cases, initial circular binaries are justified by the effect of tides. The SEVN simulations used in this work implement the tides following the formalism by [Hurley et al. \(2002\)](#) (see also [Iorio et al. 2023](#)) and show that for *Gaia* BH3-like systems, tides are extremely inefficient. The tidal efficiency is at its maximum after the main-sequence phase of the BH progenitor, when the star expands and develops a convective envelope. Assuming that the dominant tidal dissipation mechanism is due to convective motions in the envelope ([Zahn 1977](#); [Hurley et al. 2002](#)) and considering the MIST models at $Z = 4.1 \times 10^{-5}$ (Fig. 1), we estimated a circularisation timescale due to tides of $\tau_{\text{circ}} \approx 10^{25}\text{--}10^{38}$ Gyr. This timescale is orders of magnitude longer than the lifetime of the binary system and especially longer than the post main-sequence phase, when tides are more efficient.

4.3. Systematic uncertainties

Table 1 shows that the formation efficiency of BH-star systems drops significantly for models with high supernova kicks. In the models VK100 and VK265, we can exclude the hypothesis that the observation of *Gaia* BH3 is consistent with the isolated channel at a high level of significance ($>3\sigma$). Estimates of BH kicks

rely on a few tracers (e.g. X-ray binaries) and are subject to many uncertainties and systematics (see, e.g., [Andrews & Kalogera 2022](#); [Atri et al. 2019](#); [Shenar et al. 2022a](#)). The association of *Gaia* BH3 with a stellar stream ([Balbinot et al. 2024](#)) indicates that the binary system did not experience a kick much higher than the typical escape velocity from a star cluster (<10 km/s) at the time of BH formation (Sect. 3.4).

In our analysis, we did not consider binaries with companion stars less massive than $0.71 M_{\odot}$. As discussed by [El-Badry \(2024\)](#), such a population can represent a significant portion of the stellar companions of *Gaia* BH3-like systems. To assess the relevance of this population on the estimate of the formation efficiency, we generated new initial conditions, as done in Sect. 2.1, but we assumed an extended mass ratio range from $0.08 M_{\odot}/m_1$ to 1. We find that the percentage of binaries hosting a BH progenitor and a secondary star less massive than $0.71 M_{\odot}$ is 40% of similar binaries with a secondary in the mass range $0.71\text{--}1.0 M_{\odot}$. Therefore, we expect an overall increase in the formation efficiency by about 40% with respect to the value reported in Table 1. This factor is balanced by the commonly assumed binary fraction in stellar populations (40–60%; see, e.g., [Moe & Di Stefano 2017](#)).

Many population synthesis studies on BH-star binaries are based on stellar evolution models by [Pols et al. \(1998\)](#) (see, e.g., [Breivik et al. 2017](#); [Shao & Li 2019](#); [Olejak et al. 2020](#); [Chawla et al. 2022](#); [Shikauchi et al. 2023](#); [Di Carlo et al. 2024](#)). In general, the stars in these tracks tend to expand to larger radii compared to the MIST models. Most of these works focus on the Galactic population, of which the stellar halo is a negligible component. Hence a direct comparison is not straightforward. We note that the properties of the few metal-poor stars reported by [Chawla et al. \(2022\)](#) and the halo population discussed by [Olejak et al. \(2020\)](#) seem to be qualitatively consistent with the distribution of the BH-star systems found in our simulations in terms of period and companion mass.

[Di Carlo et al. \(2024\)](#) report a BH star formation efficiency for the isolated channel at least one order of magnitude lower than what we found in our simulations. Moreover, these authors claim that any BH-star system with an eccentricity larger than 0.5 and a BH mass larger than $30 M_{\odot}$ are exclusively associated with the dynamical formation channel. The origin of this discrepancy is twofold. First, their sample is dominated by the metal-rich population of the Milky Way disc. Secondly, their stellar and binary evolution models are significantly different from the ones adopted in this work. In particular, [Di Carlo et al. \(2024\)](#) used stellar tracks by [Pols et al. \(1998\)](#) and a different supernova and natal kick model.

The number of binaries simulated in our models correspond to a stellar population with a total mass of $\sim 10^9 M_{\odot}$. This mass is representative of the old and metal-poor Galactic stellar halo ([Deason et al. 2019](#)). However, a single halo realisation suffers from stochastic fluctuations. The model fiducial2E8, in which we simulated 2×10^8 binaries, indicates that our fiducial model slightly underestimates the number of *Gaia* BH3-like binaries (Table 1). However, by dividing the initial conditions of fiducial2E8 (Sect. 2.3) into sub-samples of 2×10^7 binaries, we are able to confirm that the errors quoted in Table 1 realistically capture the uncertainties.

4.4. Alternative formation channel

Gaia BH3 is associated with the ED-2 stream ([Balbinot et al. 2024](#)). Therefore, it possibly spent a part of its life in a dynamical environment. The variety of interactions in dynamical

environments has two competitive effects. On the one hand, they can pair BHs and stars or create binary systems with orbital properties (e.g. high eccentricities) that boost the production of *Gaia* BH3-like binaries. On the other hand, dynamical interactions could destroy original and newly formed BH-star systems, especially if their orbit is wide and the companion is a low-mass star.

The other two BH-star systems retrieved from *Gaia* data (BH1, El-Badry et al. 2023b; Chakrabarti et al. 2023, and BH2, El-Badry et al. 2023a) are difficult to reconcile with isolated binary evolution models (El-Badry et al. 2023a). However, they are more easily formed in star clusters (Rastello et al. 2023; Di Carlo et al. 2024; Tanikawa et al. 2024, but see Kotko et al. 2024).

Marín Pina et al. (2024) show that BH-star systems dynamically form in an efficient way in globular clusters with mass 10^5 – $10^6 M_{\odot}$. They estimated a formation efficiency of 10^{-5} – $3 \times 10^{-4} M_{\odot}^{-1}$ by considering all the BH-star systems formed in their Monte Carlo simulations (both escaped or retained in the cluster). Di Carlo et al. (2024) estimate a formation efficiency of $1.8 \times 10^{-5} M_{\odot}^{-1}$ by considering star clusters in the mass range 10^3 – $3 \times 10^4 M_{\odot}$; Rastello et al. (2023) show that the formation efficiency rises up to $\approx 10^{-3} M_{\odot}^{-1}$ for low-mass clusters ($\approx 10^2$ – $10^3 M_{\odot}$) at high metallicity ($Z = 0.02$). Assuming a mass of the ED-2 cluster progenitor in the range $\sim 10^3$ – 10^4 (Balbinot et al. 2024), the dynamical channel is one to two orders of magnitude more efficient than the isolated channel presented in this work. However, when considering the mass of the halo (Deason et al. 2019) and the cluster radial profile (e.g. Gieles & Gnedin 2023), the difference on the expected formation efficiency of BH-star systems in the solar neighbourhood reduces to a factor of three to ten between the isolated and star cluster scenario.

When focusing specifically on *Gaia* BH3-like systems, Marín Pina et al. (2024) find that only 0.6% of their BH-star systems (nine out of 1435) fall within the same selection box used in our work (Fig. 2), and only two of them (0.1%) are candidates to be within an ED2-like stream at the present time (i.e. they experience a late ejection or are still in the cluster at the end of the simulation; Marín Pina, private communication). This fraction is a factor of two to ten smaller than what we found in our fiducial model (see Table 1) when considering only old *Gaia* BH3-like systems that received a low natal kick (Table 1). Therefore, the ratio between the dynamical to isolated formation efficiency ranges from 0.6 (isolated channel slightly favoured) to 90 (dynamical channel strongly favoured). Considering the model with the higher *Gaia* BH3-like formation efficiency (ICthermal; see Table 1), the ratio ranges from 0.1 (isolated formation channel favoured) to 20 (dynamical formation channel favoured). Marín Pina et al. (2024) selected *Gaia* BH3-like systems using a wider eccentricity range: from 0.5 to 0.9. With this selection criterion, the number of *Gaia* BH3-like systems approximately doubles, yet the ratio between the isolated and dynamical channels remains unchanged. Taken at face value, these numbers seem to indicate that although the dynamical channel has an overall higher likelihood to form *Gaia* BH3, we cannot rule out the possibility that the system is compatible with a primordial binary star that escaped from the ED2 cluster.

A more quantitative comparison and model selection would require a detailed analysis of systematics, including stellar evolution models, selection effects, channel definitions, and halo population models (see e.g. Di Carlo et al. 2024). Additionally, the use of robust statistical tools is essential, as highlighted by

studies such as Mould et al. (2023). However, these aspects are beyond the scope of this paper.

5. Summary

We have explored the formation of *Gaia* BH3 (Gaia Collaboration 2024), a non-interacting binary system composed of a massive BH ($\approx 30 M_{\odot}$) and a low-mass giant star ($\approx 0.8 M_{\odot}$), by means of population synthesis simulations. We have exploited the flexibility of our code SEVN (Iorio et al. 2023) to perform the first population study of BH-star systems using the MIST stellar models (Choi et al. 2016). We explored the parameter space by considering nine different metallicities, four different supernova kick models, five models for the common envelope, two models for the onset of Roche-lobe overflow, and three different sets of initial conditions. We also implemented a Bayesian sampling analysis to study the distribution of initial conditions that reproduce the observed properties of *Gaia* BH3 exactly. The main takeaways of our analysis are as follows:

- Systems such as *Gaia* BH3 represent a common product of isolated binary evolution at low metallicity ($Z < 0.01$). They form preferentially from a massive star (40 – $60 M_{\odot}$) in an initially wide ($P > 10^3$ days) and eccentric ($e > 0.6$) orbit with a low-mass companion. The progenitor binary system never underwent Roche-lobe overflow during its life;
- Our fiducial natal kick model (Giacobbo & Mapelli 2020) produces low natal kicks for *Gaia* BH3-like systems, leaving the initial orbital properties of the binary almost unchanged. The formation of *Gaia* BH3 is possible up to kicks as high as 220 km/s, but such high kicks require fine-tuning for the properties at BH formation, reducing the overall formation efficiency by about one order of magnitude, and they are not compatible with the association with a cold stellar stream;
- Focusing on systems older than 10 Gyr, we find a formation efficiency of $\eta_{\text{BHStar}} \sim 10^{-6} M_{\odot}^{-1}$ for BH-star binaries in general and $\eta_{\text{Gaia BH3-like}} \sim 4 \times 10^{-8} M_{\odot}^{-1}$ for *Gaia* BH3-like systems;
- Considering the Galactic stellar halo model by Deason et al. (2019), we expected up to ≈ 4000 BH-star systems born in the stellar halo from isolated evolution. About 20–120 of them are *Gaia* BH3-like systems in terms of mass and orbital properties.

Overall, *Gaia* BH3 is compatible with a primordial, metal-poor binary system that never evolved via Roche-lobe overflow and experienced a long, ‘boring’ life. Given its association with the ED-2 stream, *Gaia* BH3 was born in a stellar cluster but is compatible with a primordial binary star that escaped from its parent cluster without experiencing significant dynamical interactions. Unlike *Gaia* BH1 and BH2, its orbital properties are easy to explain with current stellar and binary evolution models. However, uncertainties about massive star evolution (e.g. maximum stellar radius of the BH progenitor) and natal kicks substantially affect our final results. Future detections of dormant BHs are thus crucial to set constraints on massive star and natal kick models.

Data availability

Our initial conditions and parameter files are publicly available at <https://zenodo.org/records/11617742>. The sample of BH-star systems produced in the simulations can be downloaded from <https://zenodo.org/records/11992265>, <https://>

zenodo.org/records/12188369, and <https://zenodo.org/records/12189734>.

Acknowledgements. The authors thank the anonymous referee for their suggestions that helped us to improve the manuscript. We thank Daniel Marín Pina and Pasquale Panuzzo for useful comments, and Jakub Klencki for his contribution in revising the implementation of the Klencki21 binding energy prescriptions in SEVN. GI acknowledges financial support under the National Recovery and Resilience Plan (NRRP), Mission 4, Component 2, Investment 1.4, – Call for tender No. 3138 of 18/12/2021 of Italian Ministry of University and Research funded by the European Union – NextGenerationEU. MM, ST, MD, StR, GE, EK, EL and MPV acknowledge financial support from the European Research Council for the ERC Consolidator grant DEMOBLACK, under contract no. 770017. MM, ST, StR and MPV also acknowledge financial support from the German Excellence Strategy via the Heidelberg Cluster of Excellence (EXC 2181 – 390900948) STRUCTURES. MD also acknowledges financial support from Cariparo foundation under grant 55440. AAT acknowledges support from the European Union’s Horizon 2020 and Horizon Europe research and innovation programs under the Marie Skłodowska-Curie grant agreements no. 847523 and 101103134. SaR acknowledges support from the Beatrice de Pinós postdoctoral program under the Ministry of Research and Universities of the Government of Catalonia (Grant Reference No. 2021 BP 00213). MAS acknowledges funding from the European Union’s Horizon 2020 research and innovation programme under the Marie Skłodowska-Curie grant agreement No. 101025436 (project GRACE-BH, PI: Manuel Arca Sedda). MAS acknowledge financial support from the MERAC Foundation. Part of this work was supported by the German *Deutsche Forschungsgemeinschaft*, DFG project number Ts 17/2–1. Numerical calculations have been made possible through a CINECA-INFN (TEONGRAV) agreement, providing access to resources on Leonardo at CINECA. This work has made use of data from the European Space Agency (ESA) mission *Gaia* (<https://www.cosmos.esa.int/gaia>), processed by the *Gaia* Data Processing and Analysis Consortium (DPAC, <https://www.cosmos.esa.int/web/gaia/dpac/consortium>). Funding for the DPAC has been provided by national institutions, in particular the institutions participating in the *Gaia* Multilateral Agreement.

References

- Abbott, B. P., Abbott, R., Abbott, T. D., et al. 2016a, *Phys. Rev. Lett.*, **116**, 061102
- Abbott, B. P., Abbott, R., Abbott, T. D., et al. 2016b, *Phys. Rev. Lett.*, **116**, 241102
- Abbott, R., Abbott, T. D., Abraham, S., et al. 2021, *Phys. Rev. X*, **11**, 021053
- Abbott, R., Abbott, T. D., Acernese, F., et al. 2023, *Phys. Rev. X*, **13**, 041039
- Abbott, R., Abbott, T. D., Acernese, F., et al. 2024, *Phys. Rev. D*, **109**, 022001
- Agrawal, P., Hurley, J., Stevenson, S., Szécsi, D., & Flynn, C. 2020, *MNRAS*, **497**, 4549
- Agrawal, P., Stevenson, S., Szécsi, D., & Hurley, J. 2022a, *A&A*, **668**, A90
- Agrawal, P., Szécsi, D., Stevenson, S., Eldridge, J. J., & Hurley, J. 2022b, *MNRAS*, **512**, 5717
- Andrews, J. J., & Kalogera, V. 2022, *ApJ*, **930**, 159
- Atri, P., Miller-Jones, J. C. A., Bahramian, A., et al. 2019, *MNRAS*, **489**, 3116
- Balbinot, E., Dodd, E., Matsuno, T., et al. 2024, *A&A*, **687**, L3
- Belczynski, K., Bulik, T., Fryer, C. L., et al. 2010, *ApJ*, **714**, 1217
- Belczynski, K., Heger, A., Gladysz, W., et al. 2016, *A&A*, **594**, A97
- Bell, E. F., Zucker, D. B., Belokurov, V., et al. 2008, *ApJ*, **680**, 295
- Breivik, K., Chatterjee, S., & Larson, S. L. 2017, *ApJ*, **850**, L13
- Bressan, A., Marigo, P., Girardi, L., et al. 2012, *MNRAS*, **427**, 127
- Casaes, J., Negueruela, I., Ribó, M., et al. 2014, *Nature*, **505**, 378
- Chakrabarti, S., Simon, J. D., Craig, P. A., et al. 2023, *AJ*, **166**, 6
- Chawla, C., Chatterjee, S., Breivik, K., et al. 2022, *ApJ*, **931**, 107
- Chen, Y., Bressan, A., Girardi, L., et al. 2015, *MNRAS*, **452**, 1068
- Choi, J., Dotter, A., Conroy, C., et al. 2016, *ApJ*, **823**, 102
- Claeys, J. S. W., Pols, O. R., Izzard, R. G., Vink, J., & Verbunt, F. W. M. 2014, *A&A*, **563**, A83
- Costa, G., Bressan, A., Mapelli, M., et al. 2021, *MNRAS*, **501**, 4514
- Costa, G., Mapelli, M., Iorio, G., et al. 2023, *MNRAS*, **525**, 2891
- Deason, A. J., Belokurov, V., & Sanders, J. L. 2019, *MNRAS*, **490**, 3426
- Di Carlo, U. N., Agrawal, P., Rodriguez, C. L., & Breivik, K. 2024, *ApJ*, **965**, 22
- Eggleton, P. P. 1983, *ApJ*, **268**, 368
- El-Badry, K. 2024, *Open J. Astrophys.*, **7**, 38
- El-Badry, K., Rix, H.-W., Cendes, Y., et al. 2023a, *MNRAS*, **521**, 4323
- El-Badry, K., Rix, H.-W., Quataert, E., et al. 2023b, *MNRAS*, **518**, 1057
- Farmer, R., Renzo, M., de Mink, S. E., Marchant, P., & Justham, S. 2019, *ApJ*, **887**, 53
- Foreman-Mackey, D., Hogg, D. W., Lang, D., & Goodman, J. 2013, *PASP*, **125**, 306
- Fryer, C. L., Belczynski, K., Wiktorowicz, G., et al. 2012, *ApJ*, **749**, 91
- Gaia Collaboration (Vallenari, A., et al.) 2023, *A&A*, **674**, A1
- Gaia Collaboration (Panuzzo, P., et al.) 2024, *A&A*, **686**, L2
- Geller, A. M., Leigh, N. W. C., Giersz, M., Kremer, K., & Rasio, F. A. 2019, *ApJ*, **872**, 165
- Generozov, A., & Perets, H. B. 2024, *ApJ*, **964**, 83
- Giacobbo, N., & Mapelli, M. 2020, *ApJ*, **891**, 141
- Gieles, M., & Gnedin, O. Y. 2023, *MNRAS*, **522**, 5340
- Giesers, B., Dreizler, S., Husser, T.-O., et al. 2018, *MNRAS*, **475**, L15
- Giesers, B., Kamann, S., Dreizler, S., et al. 2019, *A&A*, **632**, A3
- Gilkis, A., Shenar, T., Ramachandran, V., et al. 2021, *MNRAS*, **503**, 1884
- Gnedin, O. Y., Zhao, H., Pringle, J. E., et al. 2002, *ApJ*, **568**, L23
- Guseinov, O. K., & Zel’dovich, Y. B. 1966, *Soviet Ast.*, **10**, 251
- Heger, A., & Woosley, S. E. 2002, *ApJ*, **567**, 532
- Hobbs, G., Lorimer, D. R., Lyne, A. G., & Kramer, M. 2005, *MNRAS*, **360**, 974
- Hurley, J. R., Tout, C. A., & Pols, O. R. 2002, *MNRAS*, **329**, 897
- Hut, P. 1981, *A&A*, **99**, 126
- Iorio, G., Belokurov, V., Erkal, D., et al. 2018, *MNRAS*, **474**, 2142
- Iorio, G., Mapelli, M., Costa, G., et al. 2023, *MNRAS*, **524**, 426
- Ivanova, N., Justham, S., Chen, X., et al. 2013, *A&A Rev.*, **21**, 59
- Klencki, J., Nelemans, G., Istrate, A. G., & Pols, O. 2020, *A&A*, **638**, A55
- Klencki, J., Nelemans, G., Istrate, A. G., & Chruslinska, M. 2021, *A&A*, **645**, A54
- Kotko, I., Banerjee, S., & Belczynski, K. 2024, *MNRAS*, submitted [[arXiv:2403.13579](https://arxiv.org/abs/2403.13579)]
- Kroupa, P. 2001, *MNRAS*, **322**, 231
- Lane, J. M. M., Bovy, J., & Mackereth, J. T. 2023, *MNRAS*, **526**, 1209
- Lennon, D. J., Dufton, P. L., Villaseñor, J. I., et al. 2022, *A&A*, **665**, A180
- Mahy, L., Sana, H., Shenar, T., et al. 2022, *A&A*, **664**, A159
- Mapelli, M., Colpi, M., & Zampieri, L. 2009, *MNRAS*, **395**, L71
- Mapelli, M., Ripamonti, E., Zampieri, L., Colpi, M., & Bressan, A. 2010, *MNRAS*, **408**, 234
- Mapelli, M., Zampieri, L., Ripamonti, E., & Bressan, A. 2013, *MNRAS*, **429**, 2298
- Mapelli, M., Spera, M., Montanari, E., et al. 2020, *ApJ*, **888**, 76
- Marín Pina, D., Rastello, S., Gieles, M., et al. 2024, *A&A*, **688**, L2
- Medina, G. E., Muñoz, R. R., Carlin, J. L., et al. 2024, *MNRAS*, **531**, 4762
- Miller-Jones, J. C. A., Bahramian, A., Orosz, J. A., et al. 2021, *Science*, **371**, 1046
- Moe, M., & Di Stefano, R. 2017, *ApJS*, **230**, 15
- Mould, M., Gerosa, D., Dall’Amico, M., & Mapelli, M. 2023, *MNRAS*, **525**, 3986
- Nguyen, C. T., Costa, G., Girardi, L., et al. 2022, *A&A*, **665**, A126
- Oëzel, F., Psaltis, D., Narayan, R., & McClintock, J. E. 2010, *ApJ*, **725**, 1918
- Olejak, A., Belczynski, K., Bulik, T., & Sobolewska, M. 2020, *A&A*, **638**, A94
- Penoyre, Z., Belokurov, V., & Evans, N. W. 2022, *MNRAS*, **513**, 2437
- Pols, O. R., Schröder, K.-P., Hurley, J. R., Tout, C. A., & Eggleton, P. P. 1998, *MNRAS*, **298**, 525
- Rastello, S., Iorio, G., Mapelli, M., et al. 2023, *MNRAS*, **526**, 740
- Ribó, M., Munar-Adrover, P., Paredes, J. M., et al. 2017, *ApJ*, **835**, L33
- Sana, H., de Mink, S. E., de Koter, A., et al. 2012, *Science*, **337**, 444
- Saracino, S., Kamann, S., Guarcello, M. G., et al. 2022, *MNRAS*, **511**, 2914
- Saracino, S., Shenar, T., Kamann, S., et al. 2023, *MNRAS*, **521**, 3162
- Sgalletta, C., Iorio, G., Mapelli, M., et al. 2023, *MNRAS*, **526**, 2210
- Shao, Y., & Li, X.-D. 2019, *ApJ*, **885**, 151
- Shenar, T., Sana, H., Mahy, L., et al. 2022a, *Nat. Astron.*, **6**, 1085
- Shenar, T., Sana, H., Mahy, L., et al. 2022b, *A&A*, **665**, A148
- Shikauchi, M., Tsuna, D., Tanikawa, A., & Kawanaka, N. 2023, *ApJ*, **953**, 52
- Spera, M., & Mapelli, M. 2017, *MNRAS*, **470**, 4739
- Spera, M., Mapelli, M., & Bressan, A. 2015, *MNRAS*, **451**, 4086
- Spera, M., Mapelli, M., Giacobbo, N., et al. 2019, *MNRAS*, **485**, 889
- Tanikawa, A., Susa, H., Yoshida, T., Trani, A. A., & Kinugawa, T. 2021, *ApJ*, **910**, 30
- Tanikawa, A., Hattori, K., Kawanaka, N., et al. 2023, *ApJ*, **946**, 79
- Tanikawa, A., Cary, S., Shikauchi, M., Wang, L., & Fujii, M. S. 2024, *MNRAS*, **527**, 4031
- Thompson, T. A., Kochanek, C. S., Stanek, K. Z., et al. 2019, *Science*, **366**, 637
- Trimble, V. L., & Thorne, K. S. 1969, *ApJ*, **156**, 1013
- Webbink, R. F. 1984, *ApJ*, **277**, 355
- Woosley, S. E. 2017, *ApJ*, **836**, 244
- Woosley, S. E. 2019, *ApJ*, **878**, 49
- Xu, X.-J., & Li, X.-D. 2010, *ApJ*, **722**, 1985
- Zahn, J. P. 1977, *A&A*, **57**, 383
- Zampieri, L., & Roberts, T. P. 2009, *MNRAS*, **400**, 677
- Ziosi, B. M., Mapelli, M., Branchesi, M., & Tormen, G. 2014, *MNRAS*, **441**, 3703